

A code for optically thick and hot photoionized media

Anne-Marie Dumont¹, Arnaud Abrassart¹, Suzy Collin¹

¹Observatoire de Paris, Section de Meudon, Place Janssen, F-92195 Meudon, France

Received 1999; accepted ...

Abstract. We describe a code designed for hot media ($T \geq$ a few 10^4 K), optically thick to Compton scattering. It computes the structure of a plane-parallel slab of gas in thermal and ionization equilibrium, illuminated on one or on both sides by a given spectrum. Contrary to the other photoionization codes, it solves the transfer of the continuum and of the lines in a two stream approximation, without using the local escape probability formalism to approximate the line transfer. We stress the importance of taking into account the returning flux even for small column densities (10^{22} cm $^{-2}$), and we show that the escape probability approximation can lead to strong errors in the thermal and ionization structure, as well as in the emitted spectrum, for a Thomson thickness larger than a few tenths. The transfer code is coupled with a Monte Carlo code which allows to take into account Compton and inverse Compton diffusions, and to compute the spectrum emitted up to MeV energies, in any geometry. Comparisons with CLOUDY show that it gives similar results for small column densities. Several applications are mentioned.

Key words: Radiative transfer, Galaxies:active, Ultraviolet:galaxies, X-rays:galaxies

1. Introduction.

A number of codes were built in the past to compute the structure and the emission of photoionized media. With time, these codes became more and more sophisticated, and able to treat a larger number of situations. In the sixties they were specially designed for planetary nebulae and HII regions, i.e. for dilute and optically thin media (except in the Lyman continuum) ionized by the thermal radiation of a hot star, and were rapidly used also for ionization by a non thermal continua extending in the X-ray range, i.e. for

Send offprint requests to: Anne-Marie Dumont (Observatoire de Meudon)

the Narrow Line Region of Active Galactic Nuclei (AGN). At the same time another generation of codes was developed for optically thin hot collisionally ionized media, and used for the solar corona, for supernova remnants, and for the hot intergalactic gas. At the end of the seventies, observations of compact X-ray sources implying the presence of a Thomson thick medium incited Ross (1979) to develop a radiative transfer method for the continuum using a modified version of the Kompaneets equation. In the same paper he introduced the so-called “escape probability” approximation to take into account diffusion and absorption into the lines. This approximation was thereafter amply used for the Broad Line Region: this was the beginning of the local escape probability era, with the fiducial paper of Kwan & Krolik (1981) aimed at studying the Broad Line Region of AGN (BLR), immediately followed by a similar computation for the atmospheres of X-ray binary stars (Kallman and McCray 1982) from which XSTAR derived. The most popular of these codes is CLOUDY, designed by Ferland (cf. for instance Ferland & Rees 1988) and continuously updated since this time (cf. Ferland 1996, Ferland et al. 1998). These codes are not only used for relatively “cold” clouds like the BLR, but also for warm photoionized media (Broad Absorption Line region in quasars and “Warm Absorbers” in AGN, shock heated media, etc...).

At the other extreme (i.e. for dense, non irradiated, and semi-infinite media) model atmosphere codes have been developed since the fifties with an emphasis put onto the computation of line transfer, which was treated completely, but with the LTE approximation. Non LTE effects were introduced in the sixties, and extensively studied in the seventies, with the state of the art being beautifully exposed in Mihalas book (1978). Since this time many improvements have been made in the numerical methods, in particular aiming at taking into account a large number of atoms and levels, cf. for introductory reviews Rutten 1995, Hubeny 1997.

In the nineties appeared the urgent need for “intermediate” codes, valid for thick or semi-infinite dense media, eventually hot, irradiated by a non thermal continuum

extending in the hard X-rays, to cover the whole range of situations encompassed in AGN and in binary stars. Several codes were then built, mainly to compute the emission spectrum of accretion disks, irradiated or not by an X-ray continuum. For irradiated disks, they were either of “photoionization type”, using the Kompaneets equation (Ross & Fabian, 1993, based on the Ross 1979 code), or coupling an existing photoionization code to a Monte Carlo computation (Zycki et al. 1994), to take into account Compton diffusions. On the other hand, sophisticated model atmosphere codes were transformed to be applied to accretion disk structure and emission (Hubeny, 1990, Hubeny & Hubeny 1997 and 1998), but without the external irradiation by an X-ray continuum.

Owing to the high optical thickness of the medium in several frequency ranges, such codes require that the transfer of both the continuum and the lines be solved in an “exact” way, i.e. avoiding approximations such as local escape approximation (for the lines) or one stream approximation (for the continuum). Since the medium is generally dense and sometimes close to LTE, they require that all processes and inverse processes be carefully handled. Being irradiated by an X-ray continuum, the medium contains a large number of ionic species, from low to high ionization, which should all be introduced in the computation. Finally, the medium being hot and thick, not only Thomson, but also Compton scattering, should be taken into account.

We have undertaken to build a code in order to satisfy these requirements. Precisely we have built several interconnected codes, which allow more flexibility. The ensemble is far from being perfect and still contains several approximations which restrict its use, but we intend to improve it in the future.

We have presently four codes. One of them (TITAN) is designed to study the structure of a warm or hot thick photoionized gas, and to compute its emission - reflection - transmission spectrum from the infrared up to about 20 KeV. It solves the energy balance, the ionization and the statistical equilibria, the transfer equations, in a plane-parallel geometry, for the lines and continuum. Then, given the thermal and ionization stratification, the computation of the emitted spectrum from 1 KeV to a few hundred KeV is performed with NOAR which uses a Monte-Carlo method taking into account direct and inverse Compton scattering (it allows also to study various geometries). PEGAS addresses the case of more diluted and thin media, and is similar to CLOUDY with however some differences, and IRIS is specially devoted to the computation of the line fluxes, including very weak lines, using the most recent available atomic data and a full treatment of the statistical equilibrium equations for a great number of levels. These codes can be used to model a wide variety of astrophysical media, particularly those in which the energy transport is purely radiative, but also plasmas heated by other mechanisms (viscosity, shocks, energetic particles...). They have

already been used in several published papers (Collin-Souffrin et al. 1996, Czerny & Dumont 1998, Porquet et al. 1998, Abrassart 1999).

The three codes NOAR, PEGAS and IRIS, are described in other papers (Abrassart 2000, Dumont & Porquet 2000). In this paper we present TITAN and we discuss a few simple cases, schematized by a slab of gas irradiated on one side or on both sides. As far as possible we will perform comparisons with CLOUDY in the range of parameters where both codes can be used, to assess the validity of TITAN. However detailed comparisons are not possible, as they use quite different transfer methods in particular. We will also show some examples of the capabilities of TITAN in the parameter range which is not accessible to CLOUDY.

TITAN is mainly designed to determine the structure (temperature and ionization state) and the continuum emission spectrum of a thick hot photoionized slab of gas. Owing to the representation of the ions made in the code it does not give an accurate determination of the weak lines. For a detailed determination of the line spectrum of some ions, it should be complemented by IRIS.

We briefly summarize below the physical processes (Sect. 2), the transfer method and the iteration procedure (Sect. 3), the thermal equilibrium, (Sect. 4), focussing only on the aspects which are not treated in a standard way. The coupling of TITAN and NOAR is briefly described in Sect. 5, and some applications are presented in Sect. 6.

2. Physical processes

In TITAN the physical state of the gas (temperature, ion abundances and level populations of all ionic species) is computed at each depth, assuming stationary state, i.e. local balance between ionizations and recombinations of ions, excitations and deexcitations, local energy balance (equality of heating due to absorption and cooling due to local emission), and finally total energy balance (equality between inward and outward fluxes).

Due to the large range of density and temperature inside the medium, many physical processes play a role at some place and should therefore be taken into account. Ionization equilibrium equations include radiative ionizations by continuum and line photons, collisional ionizations and recombinations, radiative and dielectronic recombinations, charge transfer by H and He atoms, the Auger effects, and ionizations by high energy electrons arising from ionizations by X-ray photons. Energy balance equations include free-free, free-bound and line cooling, and Compton heating/cooling.

The emission-absorption mechanisms for the continuum include free-free and free-bound processes, two-photon process, and Thomson scattering. Special care is given to recombinations to ground state, which are very important from an observational point of view in the X-ray range. They are treated differently according to the relative val-

ues of kT to the photon energy bin, in order to get an accurate frequency dependence.

Hydrogen and hydrogen-like ions are treated as 6-level atoms. Levels 2s and 2p are treated separately, while full l-mixing is assumed for higher levels. All processes including collisional and radiative ionizations and recombinations are taken into account for each level (cf. Mihalas 1978). Recombinations onto levels $n > 5$ are not taken into account, which amounts to assuming that the higher levels are in LTE with the continuum, which is generally true in the conditions for which this code is presently used. In the future we plan to add several other levels, and to sum the contributions of the higher levels as it is done for instance in CLOUDY. Level populations are then obtained as usual by matrix inversion.

In order to save computation time, non H-like ions are presently treated with a rough approximation: interlocking between excited levels is neglected and populations of the excited levels are computed separately using a two-level approximation. This approximation does not predict correctly the details of the line spectrum, since it neglects subordinate lines. Nevertheless recombinations onto excited states are taken into account in the ionization equilibrium and the transfer of these photons is treated in an approximative way as proposed by Canfield & Ricchiazzi (1980). We assume also that each recombination produces a resonant photon after cascades.

The gas composition include 10 elements (H, He, C, N, O, Ne, Mg, Si, S, Fe), and all their ionic species are taken into account. Photoionization cross sections are fitted from Reilman & Manson (1979) and Band L.M. et al. (1990), these values being correct as far as neutral and once ionized ions are not concerned, and it is the case in hot media. For total radiative and dielectronic recombination rates, we use Aldrovandi & Péquignot's data (1973). When possible, collisional excitation rates are taken from the Daresbury Report (1985). Most of data for iron come from Arnaud & Raymond (1992), Kaastra & Mewe (1993), and from Fuhr et al. (1988). Ionizations by high energy electrons arising from ionizations by X-range photons are taken from Bergeron & Souffrin (1973). Inverse processes (except dielectronic recombinations) are computed through the equations of detailed balance. In the case of a gas close to LTE, we neglect dielectronic recombinations for consistency to insure the balance for each process. All induced processes are taken into account.

The equations are not recalled as they have been given in previously quoted papers.

Iron K lines

These lines require special attention as they are intense in Seyfert nuclei, and they will be observed in detail in the future with Chandra and XMM. Though the iron K lines constitute a complex system described in Band D.L. et al. (1990), we assume presently only one “mean” line per ion with an oscillator strength equal to 0.4, as suggested

by Band. More detailed computations are not required as far as the Doppler broadening of the lines (or Compton broadening as well, see Abrassart 2000) is much larger than the distance between the lines, as it is the case in AGN.

In other computations of the line fluxes it is generally assumed that resonant trapping of $K\alpha$ photons of FeXVII to Fe XXIII (Ross & Fabian 1993) suppress completely these lines when the Thomson thickness of the emitting medium is larger than a given value, of the order of 0.02 (Zycki & Czerny 1994). Here the transfer of these lines is handled in a standard way, with an additional term included in the statistical and ionization equations to take into account the competition between radiative deexcitation and the Auger process. The population N_i^k of the upper level of a transition $K\alpha$ of the ion i is given by:

$$N_i^k A_{ki} = y_{i-1} (N_{i-1} K_{i-1} + N_i B_{ik} J_{ik}) \quad (1)$$

while the ionization equation for the same ion i writes:

$$\begin{aligned} N_i [(P_i + K_i) + B_{ik} J_{ik} (1 - y_{i-1})] \\ = N_{i+1} \alpha_i - N_{i-1} K_{i-1} (1 - y_{i-1}). \end{aligned} \quad (2)$$

A_{ki} and B_{ik} are the Einstein coefficients of the $K\alpha$ line, J_{ik} is the mean intensity integrated over the line profile, y_i is the fluorescent yield, α_i is the recombination coefficient, and P_i (respt. K_i) is the photoionization rate of the ground state (respt. of the K-shell) of the ion i . The second term on the left side of Eq. 2 is generally only of the order of 10% of the total photoionization rate.

3. Radiation transfer

An important quantity will be used all along this paper, the illumination (or “ionization”) parameter. Among several definitions used in the literature, we adopt the following:

$$\xi = \frac{4\pi F_{\text{inc}}}{n_{\text{H}}}, \quad (3)$$

where F_{inc} is the frequency integrated flux incident on one side of the slab and n_{H} is the hydrogen number density at this surface. Note that it does not preclude the possibility of having also a flux incident on the back side of the slab. We call the attention on the fact that all along this paper we will **mimic** a semi-isotropic and not a mono-directional illumination.

3.1. Present method for the transfer of the continuum

We want to study, on one hand media with an optical thickness larger than unity in a range of frequency rich in emission or in absorption lines, on the other hand media with a very inhomogeneous structure. For instance if the illuminated side has a temperature of a few 10^6 K, while

the temperature is only a few 10^4 K on the back side of the cloud, the spectrum emitted by the illuminated side is mainly formed in hot layers where the absorption coefficient is weak at all wavelengths and Thomson diffusion is dominant (we shall call it the “**reflected spectrum**” **though it does not correspond to pure reflection**). On the contrary the spectrum emitted by the backside of the slab is formed in cold layers where absorption must be carefully taken into account (we shall call it the “**outward spectrum**”). Note also that, even if the incident illumination is mono-directional, the “**transmitted spectrum**” is almost isotropic since the Thomson thickness, τ_T , is larger than unity. It is therefore not differentiated from the “**outward spectrum**” even when the incident source is not located on the line of sight. It is possible to estimate an approximate transmitted spectrum using the expression $F_\nu^{\text{transm}} = F_\nu^{\text{inc}} \exp(-\tau_\nu)$, where F_ν^{inc} is the incident flux, in an aim of comparison.

The transfer is treated with the Eddington two-stream approximation, i.e. the intensity is assumed to be constant in each hemisphere. The transfer equations can then be written :

$$\begin{aligned} \frac{1}{\sqrt{3}} \frac{dI_\nu^+}{dz} &= -(\kappa_\nu + \frac{\sigma}{2})I_\nu^+ + \frac{\sigma}{2}I_\nu^- + \epsilon_\nu & (4) \\ \frac{-1}{\sqrt{3}} \frac{dI_\nu^-}{dz} &= -(\kappa_\nu + \frac{\sigma}{2})I_\nu^- + \frac{\sigma}{2}I_\nu^+ + \epsilon_\nu \end{aligned}$$

where z is the distance to the illuminated edge, κ_ν is the absorption coefficient, σ is the diffusion coefficient - here it is due to Thomson scattering - and ϵ_ν is the emissivity (all these quantities are local and depend on the frequency ν except σ). Note that this approximation is closer to the semi-isotropic case than to the normal case. We have already mentioned that it is appropriate for the reflected and for the transmitted flux when the Thomson thickness is larger than unity. It is also appropriate for a semi-isotropic illumination, if the source of radiation is extended (like for instance in the disk-corona model of AGN, or in the blob model of Collin-Souffrin et al. 1996).

The mean intensity J_ν is equal to $(I_\nu^+ + I_\nu^-)/2$, while the flux F defined as usual by $\int I_\nu \cos \theta d\omega$ is equal to $(I_\nu^+ - I_\nu^-) 2\pi/\sqrt{3}$; so that the reflected flux is equal to $I_\nu^-(0) 2\pi/\sqrt{3}$, and the outward flux to $I_\nu^+(H) 2\pi/\sqrt{3}$. The optical depth and the total optical depth are defined as :

$$\tau_\nu(z) = \int_0^z \sqrt{3}(\kappa_\nu + \sigma)dz' \quad \text{and} \quad T_\nu = \tau_\nu(H) \quad (5)$$

where H is the total thickness of the slab, and the source function as:

$$S = \frac{(\epsilon_\nu + \sigma J_\nu)}{(\kappa_\nu + \sigma)} \quad (6)$$

Both sides of the slab can be illuminated by an external radiation, so the boundary conditions are, at $z = 0$:

$$I_\nu^+(0) = \frac{\sqrt{3}}{2\pi} F_\nu^{\text{inc}}, \quad (7)$$

and at $z = H$:

$$I_\nu^-(H) = \frac{\sqrt{3}}{2\pi} F_\nu^{\text{back}} \quad (8)$$

where F_ν^{back} is the back-side flux (it is equal to zero in many of the following computations).

The formal solution of the transfer equations between $z - \delta z$ and z gives:

$$I_\nu^+(z) = I_\nu^+(z - \delta z)e^{-\delta\tau_\nu} + e^{-\tau_\nu} \int_{\tau_\nu - \delta\tau_\nu}^{\tau_\nu} S_\nu(t)e^{+t}dt. \quad (9)$$

Assuming that $S_\nu(t)$ is nearly constant in the interval $z, z + \delta z$, one gets:

$$I_\nu^+(z) = I_\nu^+(z - \delta z)e^{-\delta\tau_\nu} + \frac{1 - e^{-\delta\tau_\nu}}{2} [S_\nu(z - \delta z) + S_\nu(z)] \quad (10)$$

with a similar equation for $I_\nu^-(z)$.

Guessing the initial value of $I_\nu^-(0)$ fails because calculations diverge, unless this initial value is provided with an extreme precision: the predicted value should differ from the real one at all frequencies by less than 10^{-6} . This problem has also been pointed out by Coleman (1993). We therefore start to compute $I_\nu^-(z)$ from the back side with:

$$I_\nu^-(z) = I_\nu^-(z + \delta z)e^{-\delta\tau_\nu} + \frac{1 - e^{-\delta\tau_\nu}}{2} [S_\nu(z + \delta z) + S_\nu(z)] \quad (11)$$

o Thus we calculate $S_\nu(z)$ and the mean intensity $J_\nu(z)$ from Eq. 6 and:

$$\begin{aligned} J_\nu(z) &= \frac{I_\nu^+(z - \delta z) + I_\nu^-(z + \delta z)}{2} e^{-\delta\tau_\nu} & (12) \\ &+ \frac{(1 - e^{-\delta\tau_\nu})}{4} [S_\nu(z - \delta z) + 2S_\nu(z) + S_\nu(z + \delta z)] \end{aligned}$$

assuming a constant δz (actually it is not constant so the formulae are more complicated but do not deserve to be given here).

The procedure is then the following. We divide the slab into a set of plane-parallel layers with the density n_H given in each layer. Note that the code can easily be coupled with a prescription for the density or for the pressure, such as a constant pressure, or a pressure given by hydrostatic equilibrium. Presently the slab is divided in about 300 layers. The geometrical thickness of each layer is smaller close to the surfaces than in the middle of the slab because of the rapid variation of the physical parameters (the optical thickness, the temperature, the ionization state).

- For each layer, starting from the illuminated side, where $I_\nu^+(0)$ is given by Eq. 7, the ionization and thermal balance equations are solved. The source function, the opacity and the emissivity, are computed. As they depend on J_ν , we use Eq. 13 with the value of $I_\nu^+(z - \delta z)$ of the previous layer and the value of $I_\nu^-(z + \delta z)$ provided by the previous iteration and given by Eq. 11 (see below).

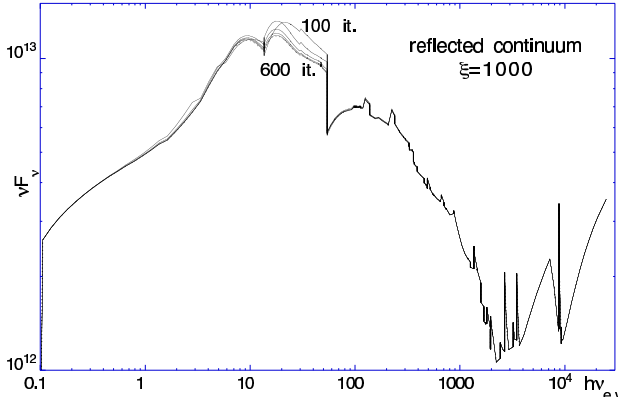


Fig. 1. The reflected continuum νF_ν , in $\text{erg cm}^{-2} \text{s}^{-1}$, after a number of iterations varying from 100 to 600, displayed all 100 iterations, for the reference model. We see that the spectrum does not vary at all after 400 iterations.

- $I_\nu^+(z)$ is transferred through the layer according to Eq. 10, while $S_\nu(z)$ and $\tau_\nu(z)$ are buffered for each layer and each frequency.

- when the back side of the cloud is reached, new values of $I_\nu^-(z)$ are calculated, starting from the back side where $I_\nu^-(H)$ is given by Eq. 8, and using Eq. 11 with the previous values of $S_\nu(z)$ and $\tau_\nu(z)$; actually we use the values given by several previous iterations to accelerate the procedure.

- the whole calculation is repeated until convergence. It is stopped when energy balance is achieved for the whole slab (i.e. when the flux entering on both sides of the slab is equal to the flux coming out from both sides).

The drawback of this method is that it requires a large number of iterations to get a complete convergence of the model. The iteration starts by assuming given values for $I_\nu^-(z)$. If this initialisation is not adequate, convergence problems are encountered. We have chosen for the first iteration $I_\nu^-(z)$ equal to $I_\nu^+(z)$ multiplied by a factor of the order of unity, which works reasonably well. Actually the convergence of $I_\nu^-(z)$ (as well as of the temperature and the ionization state) is reached within less than 1% after only a relatively small number of iterations in the layers corresponding to about one Thomson thickness. This property is interesting as far as the outward spectrum is negligible, which is the case in the EUV and X-ray range. It can also be used to determine the ionization state and the temperature of the layers where Compton diffusion takes place (cf. Sect. 5 about coupling with the code NOAR).

Fig. 1 displays the reflected continuum obtained after different numbers of iterations (for clarity we prefer to show here the continuum and not the complete spectrum). The model is a slab with the following characteristics:

- a constant density 10^{12} cm^{-3} ,
- a column density 10^{26} cm^{-2} ;

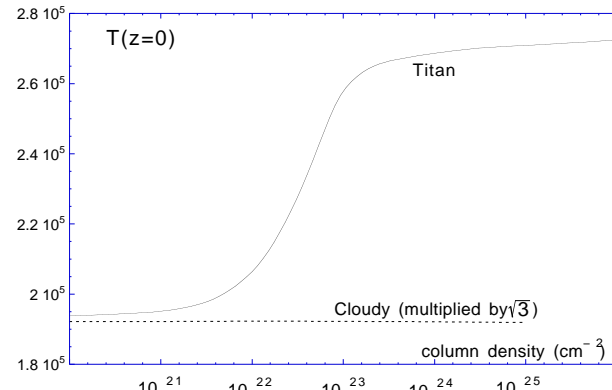


Fig. 2. Variation of the surface temperature, in K, with the column density, for a slab illuminated on one side by a power law continuum with $\xi = 100 \text{ erg cm s}^{-1}$. The surface temperature computed by CLOUDY for ξ multiplied by $\sqrt{3}$ is shown for comparison.

- it is illuminated on one side by an incident power law continuum proportional to ν^{-1} from 0.1 eV to 100 KeV,
- the illumination parameter is $\xi = 10^3 \text{ erg cm s}^{-1}$;
- there is no illumination on the other side;
- the abundances are (in number): H: 1, He: 0.085, C: $3.3 \cdot 10^{-4}$, N: $9.1 \cdot 10^{-5}$, O: $6.6 \cdot 10^{-4}$, Ne: $8.3 \cdot 10^{-5}$, Mg: $2.6 \cdot 10^{-5}$, Si: $3.3 \cdot 10^{-5}$, S: $1.6 \cdot 10^{-5}$, Fe: $3.2 \cdot 10^{-5}$.

In the following we will call this our “reference model”. All along the paper we will use the same density and the same spectral distribution of the illuminating radiation, so we will not specify these parameters anymore. Note that, for this peculiar spectral distribution, ξ and the ratio of incident ionizing photon number to hydrogen densities, U , are related by : $\xi = 8.21 U \ln(\nu_{\max}/\nu_{\min})$ where ν_{\max} and ν_{\min} are the maximum and minimum photon frequencies.

We want to stress here the importance of the backward intensity. It cannot be neglected as it participates to the ionization, to the level population, and to the energy balance. For instance in a purely scattering medium the returning flux varies as $F_{\text{inc}} \frac{\tau_T/2}{1+\tau_T/2}$, so when τ_T is much larger than unity, all the incident flux is reflected. Thus the temperature of the first layer at the illuminated side (which depends on the sum of incident plus returning radiation) should increase with the column density for a given incident flux (except possibly in cases of very high values of the illumination parameter).

Fig. 2 shows the dependence of the surface temperature on the column density N . The model is similar to the reference one except that the illumination parameter is equal to $100 \text{ erg cm s}^{-1}$ and the column density is varying. We see that the surface temperature is constant up to about $N = 10^{22} \text{ cm}^{-2}$, but after it increases from $2 \cdot 10^5 \text{ K}$ to $2.7 \cdot 10^5 \text{ K}$ for N increasing from 10^{22} to 10^{24} cm^{-2} . It saturates when a large fraction of the slab becomes close to LTE, and the returning flux becomes constant. With CLOUDY (version 9004) the surface temperature does not

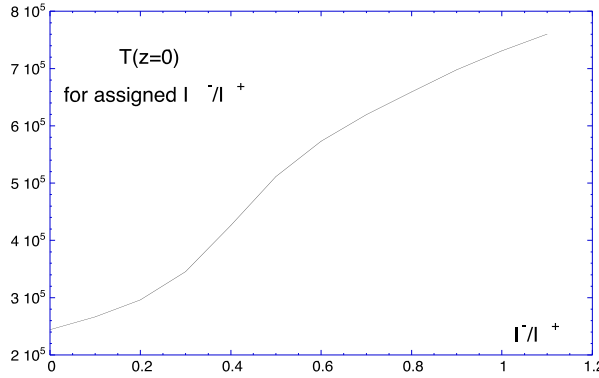


Fig. 3. Dependence of the surface temperature, in K, on the ratio $I^-(0)/I^+(0)$ imposed a priori.

depend on the column density (for a correct comparison the illumination parameter in CLOUDY must be multiplied by a factor $\sqrt{3}$ to account for the semi-isotropic approximation used in TITAN).

Fig. 3 displays the dependence of the surface temperature on an assigned ratio $I^-(0)/I^+(0)$ independent of the frequency. We see that a modest returning flux (20%) is sufficient to account for the 60% increase of the surface temperature reached for $N = 10^{24} \text{ cm}^{-2}$, with respect to a very small column density. To understand this behaviour, one should remember that the spectral distribution of the reflected flux contains a much larger proportion of EUV radiation than the incident continuum, in particular in the lines. So the illumination parameter is increased by a larger amount than the ratio of the integrated reflected over incident continuum. We can also guess that the increase of the temperature at the illuminated surface with respect to CLOUDY will be compensated by a decrease at the back side, because of energy conservation (cf. Fig. 14).

3.2. Present method for line transfer

Radiative transfer of the lines is treated in the same way as the continuum, the line profile being represented by several frequencies distributed symmetrically around the line center.

We assume that even if large macroscopic velocities are present, they do not play any role in the line transfer, in other words that the thickness of the slab is much smaller than the scale length of the velocity gradient. We also assume that the lines do not overlap, which is valid as far as multiplets are treated globally, and if the microscopic turbulent velocity is not much larger than the thermal velocity (doing this we neglect line fluorescence due to the overlap of two lines, like the HeII Balmer β line and the hydrogen Ly α line, whose wavelengths differ only by a fraction $4 \cdot 10^{-4}$).

Finally we assume presently complete redistribution in all the lines. We intend to include partial redistribution for

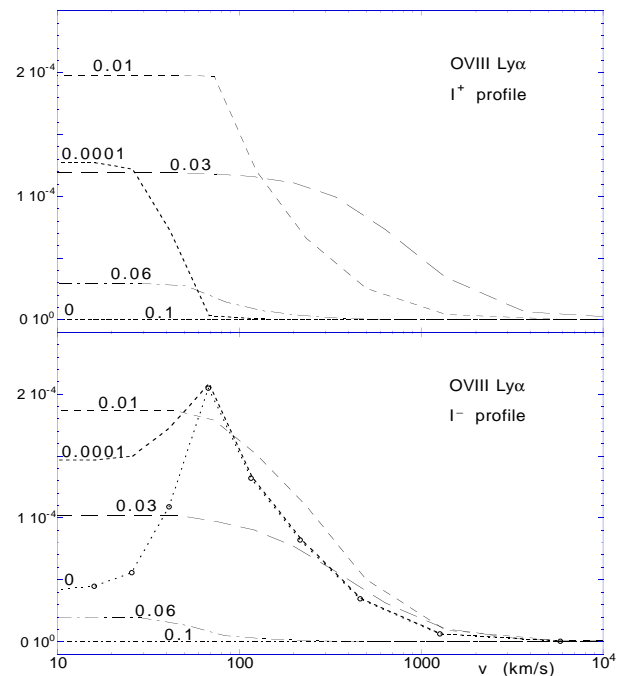


Fig. 4. Profile of I_ν^- and I_ν^+ for OVIII Ly α , for the reference model. The curves are labelled by the value of z/H .

resonance lines like Ly α in the near future. For the moment partial redistribution in these lines can be mimicked by assuming complete redistribution in a pure Doppler profile, as the line photons diffuse more in space than in frequency, owing to the absence of enlargement of the lower level. A Doppler profile can also be used for strongly interlocked lines, and in any case, it does not differ strongly from a Voigt profile when τ_0 is smaller than $1/a$ so the medium is optically thin in the damping wings. Note that partial redistribution is less important in dense media, like irradiated accretion disks in AGN, than in dilute media, owing to collisional redistribution.

The line profile ϕ_ν is a symmetrical Voigt function. The Doppler width $\Delta\nu_d$ and the damping constant depend on the temperature and on the density, and consequently vary with z . It may happen that the temperature decreases by two orders of magnitude from the illuminated to the back side, so $\Delta\nu_d$ decreases by one order of magnitude. This must be taken into account to choose the points in the profile. To solve the statistical equilibrium equations one needs to know the total line intensity weighted by the profile $\int J_\nu \phi(\nu) d\nu$, and to treat the thermal and ionization equilibria one simply integrates the line intensity over the frequencies $\int J_\nu d\nu$. For intense lines the first integral is dominated by the Doppler core, and the second by the wings. In the case of a saturated line with strong wings, the set of frequencies chosen to describe the line must cover a range from a few tenths $\Delta\nu_d$ to a few hundreds $\Delta\nu_d$ and at least 10 points are necessary for a correct representation of the profile.

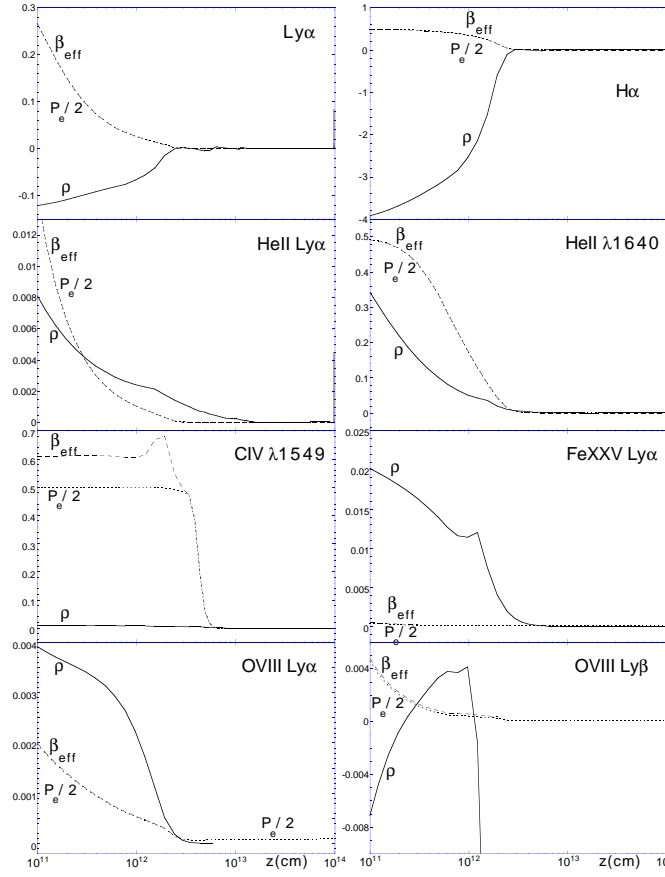


Fig. 5. Variation of ρ , $P_e(\tau_0)/2$ and β_{eff} as functions of the distance to the illuminated side for several intense lines, for the reference model.

Fig. 4 displays for the reference model the variation with z/H of the OVIII Ly α profile in both directions, I_ν^- and I_ν^+ , J_ν being the half sum of these profiles. We see that the profile varies considerably from the surface to the deeper layers.

Now we are able to show the difference between the transfer treatment and the escape probability approximation for the lines discussed in the Appendix. In this aim, we have compared the divergence flux ρ (Eq. 17) with the escape probability towards the illuminated side $P_e(\tau_0)$, and with an approximate expression proposed by Rees et al. (1989) to take into account continuum absorption in the statistical and in the energy balance equations :

$$\beta_{\text{eff}} = \frac{\kappa_c}{\kappa_c + \kappa_l} + \frac{\kappa_l}{\kappa_c + \kappa_l} \frac{[P_e(\tau_0) + P_e(T_0 - \tau_0)]}{2} \quad (13)$$

where β_{eff} is the total effective escape probability, κ_l and κ_c are the absorption coefficients respectively at the line center and in the underlying continuum, T_0 is the total optical depth of the slab at the line center, and $P_e(\tau_0)$ (respt. $P_e(T_0 - \tau_0)$) are the escape probabilities towards the illuminated (respt. the back) side.

	EW (reflected)	EW (outward)
Ly α	-1.275 Å	5.61 Å
H α	-4.44 Å	21.4 Å
HeII Ly α	9.47 Å	$6.3 \cdot 10^4$ Å
HeII 1640 Å	1.76 Å	10.4 Å
CIV 1549 Å	-4.15 Å	-11.6 Å
OIII 306 Å	0.042 Å	1230 Å
OIV 280 Å	1.07 Å	569 Å
OVI 1034 Å	1.83 Å	-1.61 Å
OVII 22 Å	0.12 Å	-
OVIII Ly α	2.08 Å	-
OVIII Ly β	-0.0012 Å	-
Fe K XXIII	-32 eV	-
Fe K XXIV	303 eV	-
FeXXV 6.7 keV	170 eV	-

Table 1. Equivalent widths of a few intense lines (negative for absorption, positive for emission) in the reflected and in the outward spectra, for the reference model.

$P_e(\tau_0)/2$ and β_{eff} have been computed with TITAN and compared to ρ in Fig. 5, as functions of the distance z to the illuminated surface, for the reference model.

We see on this figure that β_{eff} and $P_e(\tau_0)/2$ are almost always identical. It is first due to the fact that the slab is very thick, so $P_e(\tau_0)$ is much larger than $P_e(T_0 - \tau_0)$ except very close to the back side, and second because κ_c is always $\ll \kappa_l$, as all the lines displayed on the figure are intense. But β_{eff} differs considerably from ρ in the region where the lines are formed (i.e. the region where ρ is not equal to zero and where the ion is present). In particular ρ is negative in an important fraction of the line formation region for H α , Ly α , and OVIII Ly α , while β_{eff} is a positive quantity.

As a consequence the line spectrum is not correctly computed when escape probabilities are used. This can be seen on Table 1 which gives the equivalent widths (negative if the line is in absorption, positive if it is in emission) of some intense lines from both sides of the slab. Several of these lines are in absorption, either from the illuminated or from the dark side, which is impossible with the escape probability approximation.

Presently the radiative transfer is solved for 300 frequencies in the continuum from 0.01 eV to 25 keV, including all the ionization edges, and for 440 spectral lines including the fluorescence Fe K lines, the integrals over the line profiles being achieved using 15-point Gauss-Legendre quadrature, together with a change of variable.

Remarks on the convergence of the method

It is well-known that the lambda iteration method used here (actually mainly for historical reasons, because we started to build a nebular code with the line escape probability approximation) converges extremely slowly for intense lines in stellar atmospheres, and we intend to replace it by the Accelerated Lambda Iteration method as soon as possible. The convergence of J_ν is achieved after 600 iterations, for all lines except a few ones and for all continua.

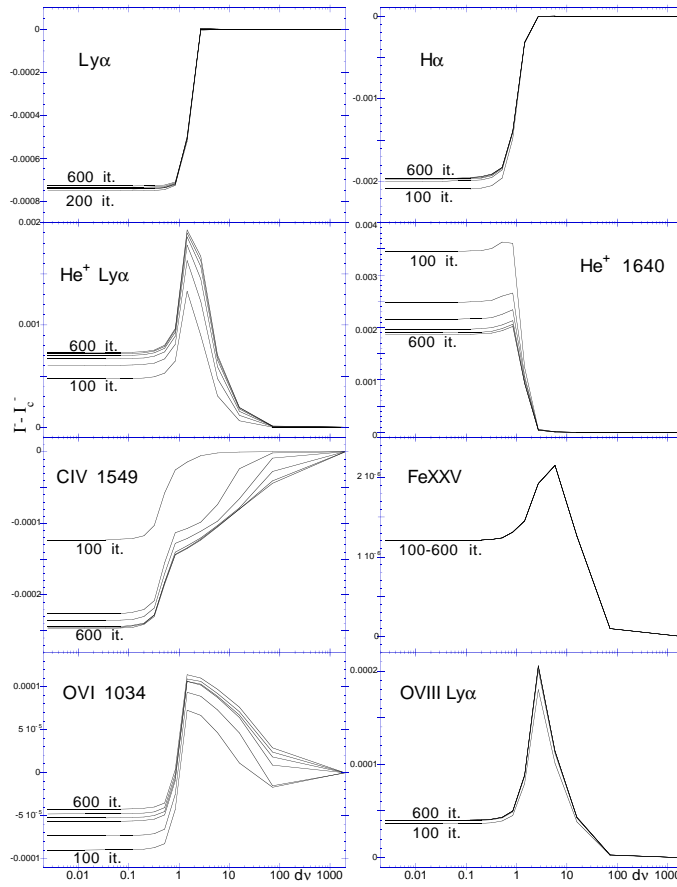


Fig. 6. Profiles of some intense lines emitted by the bright side after a number of iterations varying from 100 to 600, displayed all 100 iterations, for the reference model.

This can be checked on Fig. 6 which displays for the same lines as Fig. 5 the profiles of the lines emitted by the bright side, after different number of iterations, for the reference model. As a consequence, the structure of the slab (T , ionization) does not change at all after a few hundreds iterations. Indeed our case is more favorable than stellar atmospheres. The explanation is double: 1. the relatively small density of the medium compared to a stellar atmosphere, which decreases comparatively the influence of collisional excitations, and 2. the fact that in a photoionized plasma the temperature is low for a high ionization degree, so the excited levels lie at very high energies compared to the thermal energy. Consequently the populations of these highly ionized ions are smaller than at Boltzman equilibrium with the ground level, and the lack of convergence for excited level populations does not have a strong influence on the ionization state of the corresponding ion. We have also checked that the same structure is obtained for different initial boundary conditions. All this implies that the continuum emitted from both sides (including for instance the Lyman discontinuity) is completely converged, and only the few non converged lines are not well computed, in particular those emitted by the back side (but

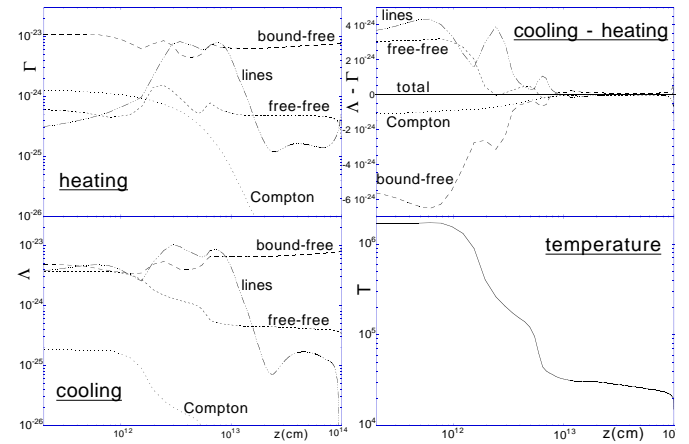


Fig. 7. Dependence of the local cooling, heating, and net cooling-heating rates, in $\text{erg cm}^{-3} \text{s}^{-1}$, and of the temperature, in K, on the distance to the illuminated side z , for the reference model.

they are negligible in the whole energy balance). Since we do not claim to compute a correct line spectrum before the subordinate lines are implemented in the code, we think that this approximation is sufficient for our present purpose.

4. Energy balance

TITAN has been designed for stationary radiatively heated media, so the energy conservation implies the balance of radiative flux. However it can be used also for other cases out of radiative equilibrium, for instance by imposing the temperature of the medium, or by adding a non radiative energy in each layer, such as the viscous flux of an accretion disk. We describe here how the code works in a purely radiative case.

We first stress the fact that the energy balance should be realized both *locally* and *globally*.

The local energy balance equation writes:

$$\int \frac{dF_\nu}{dz} d\nu = 0 = n_e n_H [-\Gamma_{\text{tot}} + \Lambda_{\text{tot}}], \quad (14)$$

where $n_e n_H \Gamma_{\text{tot}}$ and $n_e n_H \Lambda_{\text{tot}}$ are the total heating and cooling rates per unit volume. The temperature of a layer is computed through an iteration process until Γ_{tot} and Λ_{tot} are equal.

As an example, Fig. 7 gives the dependence of the cooling and heating rates, and of the equilibrium temperature, on the distance from the illuminated side z , for the reference model. We note that in this model Compton heating-cooling is not very important, and that bound-free contributes as a heating term, compensated by a cooling term due to lines and free-free processes. Note also that a quasi LTE is reached at a few Thomson depths in this model (it is reached at a smaller optical depth for a smaller value of ξ). Above this value of z the temperature

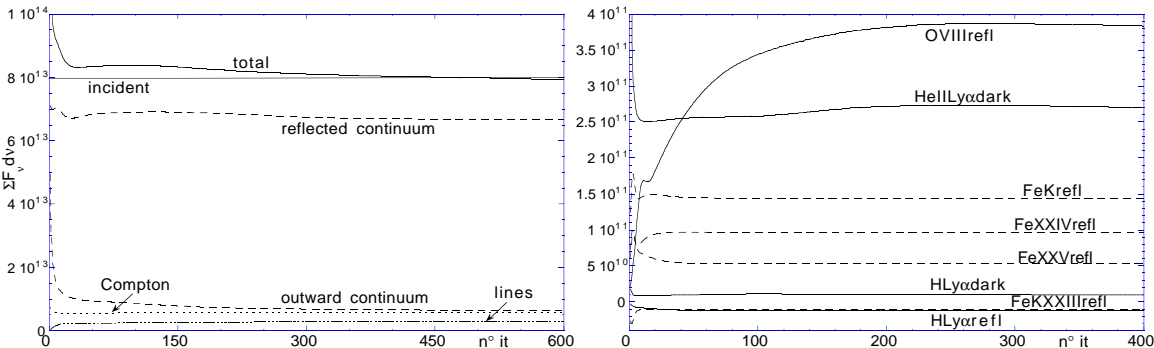


Fig. 8. Dependence of the total line and continuum fluxes and of the fluxes of a few intense lines on the number of iterations, for the reference model.

is almost constant, except close to the back side where it decreases more rapidly due to the leakage of photons.

The global energy balance is reached through an iteration procedure, when the total flux emitted by both sides of the slab, $F_{\text{tot}}^{\text{em}}$, is equal to the total flux incident on both sides, $F_{\text{tot}}^{\text{inc}}$. Actually this is the most important convergence criterium and it requires many iterations. To illustrate the problem, Fig. 8 displays the flux of a few intense emission lines and of the total flux in the lines and continuum, for the reference model, as functions of the number of iterations. We see that after about 200 iterations the global energy balance is reached within about one percent.

In the same way, Fig. 9 shows that the energy balance with TITAN is reached within one percent after 200 iterations for two models with a column density equal to 10^{25} cm^{-2} , and with an illumination parameter equal to $\xi = 100$ and $\xi = 1000 \text{ erg cm s}^{-1}$. CLOUDY or XSTAR have been used several times in this range of parameters (Martocchia & Matt, 1996, Zycki et al. 1994, for instance), but it is not sure that the global energy balance is achieved owing to the escape treatment of the lines, as discussed above.

Finally we must recall that the neglect of subordinate lines (except in hydrogen-like ions) could lead to a substantial increase of the energy losses and consequently to a change of the thermal balance, as these lines have a smaller optical thickness than resonant lines, and therefore can escape more easily from the deep layers. Since in a photoionized plasma the temperature is relatively low and the excited level populations of highly ionized ions are generally small, one could expect only a small influence on the overall spectrum.

To check this point we compare in Figs. 10 and 11 the temperature and the emitted spectrum for the reference model, with and without taking into account interlocking between excited levels in hydrogen like ions (note that interlocking is included for hydrogen and helium in both cases). These ions are the most abundant ones in the region emitting the reflected spectrum, in our refer-

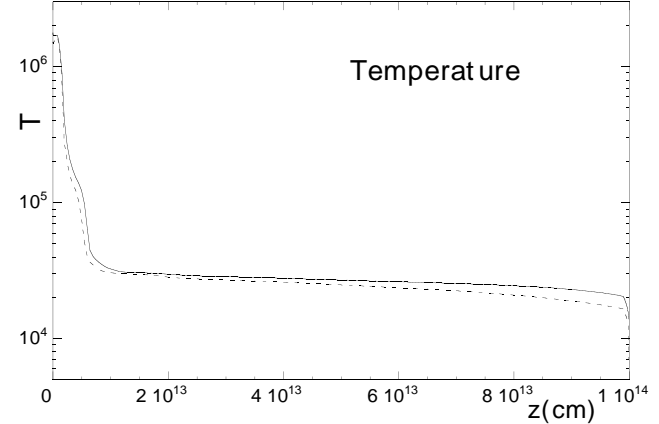


Fig. 10. Temperature in K versus z with (full line) and without (dashed lines) full five-level interlocked hydrogen-like ions, for the reference model.

ence model. Fig. 10 shows that the temperature is slightly shifted in layers corresponding to a Thomson thickness of a few. As a consequence the emitted spectrum is also different, but not by an important amount. We can infer a similar behaviour for smaller illumination parameters, even if the abundant ions are less ionized, as the temperature is also lower. For a higher illumination parameter the lines contribute less to the energy balance.

Since the detailed computed line spectrum of hydrogen-like ions is different with the two treatments, contrary to the overall spectrum, it is mandatory to treat correctly the excited levels for all the ions in order to get a correct line spectrum. Note that in this respect CLOUDY is presently doing much better than TITAN, as it includes subordinate lines and more levels for each ion.

Compton heating and cooling

The Compton heating-cooling term is equal to:

$$\Gamma - \Lambda = \frac{\sigma_T}{m_e c^2 n_H} \frac{1}{4k} (T_{\text{Comp}} - T) \int 4\pi J_\nu d\nu \quad (15)$$

where T_{Comp} is the Compton temperature. We give here this well-known equation only to recall that it depends (as

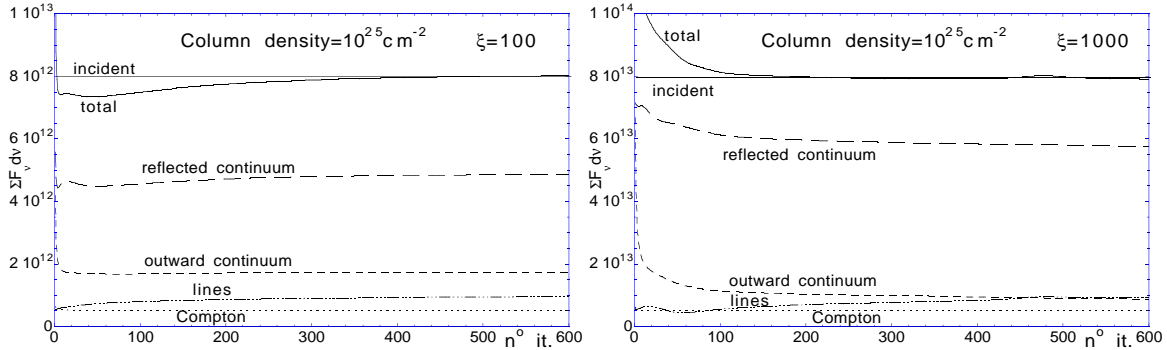


Fig. 9. Dependence of the total line and continuum fluxes on the number of iterations, for a column density of 10^{25} cm $^{-2}$, and $\xi = 10^2$ erg cm s $^{-1}$ and $\xi = 10^3$ erg cm s $^{-1}$.

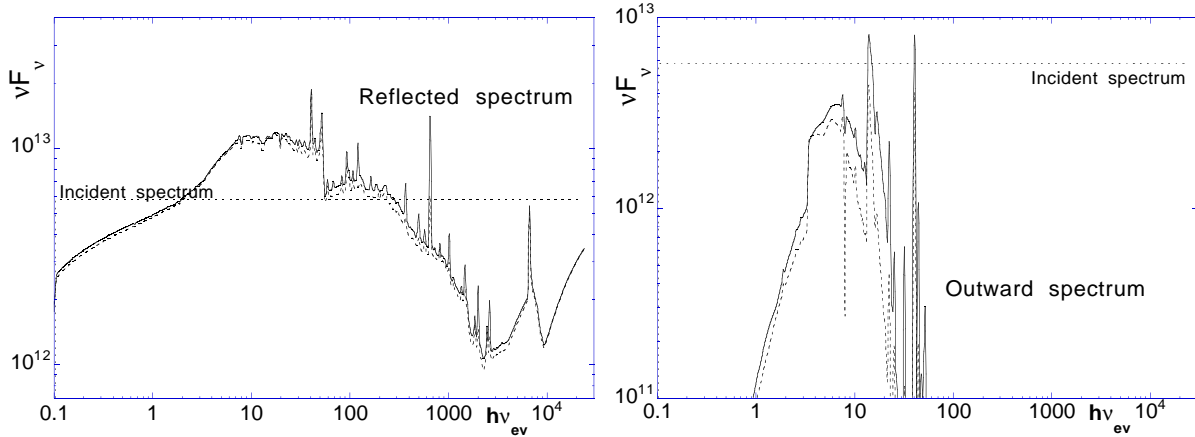


Fig. 11. Reflected and outward spectra, with (full line), and without (dashed lines) full five-level interlocked hydrogen-like ions, for the reference model. The spectra νF_ν are displayed with a line resolution of 30, in erg cm $^{-2}$ s $^{-1}$.

well as T_{Comp}) on the spectral distribution of the *local* flux, so it requires a careful computation of this flux (including the lines).

Below 25 KeV, J_ν is provided directly by TITAN in each layer. Above 25 KeV, J_ν is not calculated by TITAN, but by the code NOAR, as the energy shift of the photons due to Compton scattering is no more negligible. In this case the results from NOAR are also used to compute the exact value of the Compton heating-cooling term. This is discussed in more detail in the next section.

5. Coupling with the Monte Carlo code

In order to compute the effect of Compton scattering on the high energy part of the reprocessed radiation, and particularly on the reflected spectrum above 1 keV, and to determine precisely the Compton heating-cooling rate entering in the energy balance equation, we need another numerical approach. The transfer scheme in TITAN is based on frequency arrays, and inelastic scattering would introduce a redistribution on energy bins making the code much heavier. In this aim Abrassart (2000) developed a

Monte Carlo code, NOAR. The asset of such an approach is also that it enables to investigate an arbitrary geometry and to determine the angular dependance of the observed spectra. These aspects were difficult to tackle with a code such as TITAN. Moreover, it allows to easily extract time variability information.

NOAR is described in detail in Abrassart (2000). We explain here only how it is coupled with TITAN. It shares the same opacity data and includes the same set of 102 ions, for the 10 elements of highest cosmic abundances. Given all the ionisation degrees provided by TITAN, it computes absorption cross sections in each layer. Free-free absorption is also taken into account. NOAR includes the recombination continua of hydrogen and helium like ions, but does not include line emission, except fluorescence lines. The proper yields to account for the competition with the Auger effect are used for these lines. Fluorescence of Fe XVII-XXIII is suppressed by resonant trapping. For the pseudo fluorescence of H and He-like species, a simplifying prescription is adopted which includes only the two most probable outcomes of a K shell photoionization, i.e. direct recombination on ground level or L-K transition.

The spectral distribution of the recombination continuum is determined by the local temperature in the “current” slab.

NOAR takes into account direct and inverse Compton scattering. The method used for modelling Compton scattering is basically the one described in Pozdniakov, Sobol & Sunyaev (1983) and in Gorecki & Wilczewski (1984), with a different use of statistical weight, because of the competition with photoelectric absorption. When the high energy cut-off of the incident continuum is of the order of 100 KeV, the reflected spectrum above 10 KeV exhibits a “Compton hump” peaking at about 30 KeV (Lightmann & White 1988). This spectral region of optimal continuum albedo occurs where the sum of photoelectric absorption and Compton losses is minimum. This feature depends weakly on the ionization state, although its prominence in an observed X-ray spectra, and notably its level with respect to the iron line, is sensitive to ξ (see Fig. 19) as the soft X-ray albedo. Note that the shape and extension of the hump depends on the high energy cut-off of the incident spectrum, which is 100 KeV all along this paper.

Fluorescent lines are significantly Compton broadened for rather high illumination parameter, above $\xi \sim 10^3$ erg cm s $^{-1}$. The broadening is asymmetric, the profile is skewed toward the red. At still higher ξ and temperature, a blue wing appears, due to the inverse Compton effect. The extend and importance of both wings depends on the optical depth of the scattering medium. The red wing depends only on the frequency of the line (i.e. on the ionization state of iron) whereas the blue one only depends on the temperature of the scattering medium.

TITAN and NOAR lead to almost identical reflected spectra in the 1-20 KeV range (they differ only by Compton broadening of lines and of photoelectric edges), and NOAR allows to obtain the spectrum in the higher energy range. This spectrum is used for the global energy balance.

Another use of NOAR is to provide TITAN with the local Compton gains and losses in each layer. This is necessary, because Compton heating-cooling is dominated by energy losses of photons > 25 Kev, in particular for high values of ξ when Compton heating-cooling is dominating the energy balance and should be computed in an exact way.

As an example Fig. 12 gives the dependence of the ratio $(\Gamma_{\text{Comp}} - \Lambda_{\text{Comp}})/\xi$ on the Thomson depth, for different values of ξ , the other parameters being the same as in the reference model. We see that the ratio does not depend on the illumination parameter if $\xi \leq 10^4$ erg cm s $^{-1}$. This is expected since the Compton heating-cooling is dominated by high energy photons, which do not care about the ionization state. It also means that inverse Compton is negligible as a cooling process (though it has an influence on the line spectrum), otherwise $\frac{\Gamma - \Lambda}{\xi}$ would depend on the gas temperature and therefore on ξ . This is due to the relatively low temperature of the gas compared to the mean energy of the photons. This property breaks for very high illumination parameters, since low energy ph-

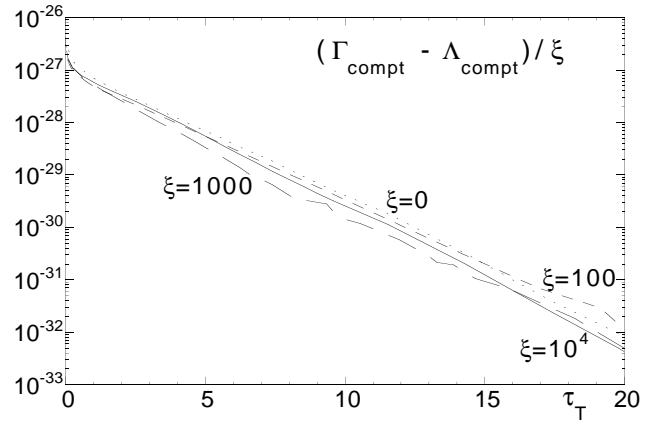


Fig. 12. Dependence of the ratio $\frac{\Gamma_{\text{Comp}} - \Lambda_{\text{Comp}}}{\xi}$ on the Thomson depth, for different values of ξ in erg cm s $^{-1}$, the other parameters being the same as in the reference model.

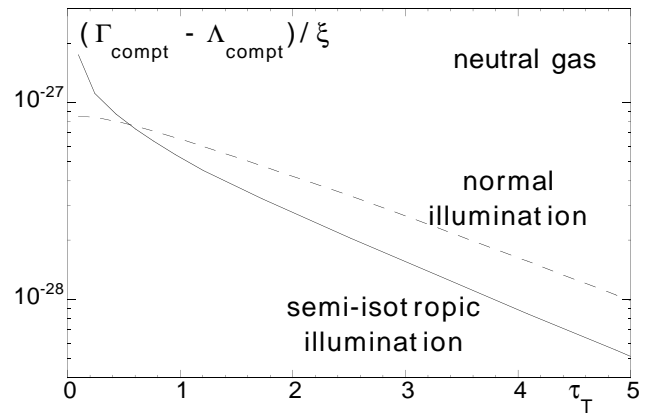


Fig. 13. Dependence of the ratio $\frac{\Gamma_{\text{Comp}} - \Lambda_{\text{Comp}}}{\xi}$ on the Thomson depth, for a neutral gas and for an isotropic or perpendicular illumination. Except ξ the parameters are the same as in the reference model.

tons are then able to penetrate in the deepest layers and to play a role in the cooling rate, and the temperature of the gas is close to T_{Comp} .

The deposition of energy shown on Fig. 12 corresponds to a semi-isotropic distribution of the incident radiation. It is different in the case of a mono-directional radiation. This is shown on Fig. 13 which displays $(\Gamma_{\text{Comp}} - \Lambda_{\text{Comp}})/\xi$ for a neutral gas in the case of an isotropic and of a perpendicular illumination. When the radiation field is semi-isotropic there is a rapid decrease of $\frac{\Gamma - \Lambda}{\xi}$ for small values of τ_T , due to the small distance covered by the photons. This is compensated by a smaller (by about a factor two) deposition of energy in the deeper layers.

The Compton heating-cooling rate obtained with NOAR is then fitted analytically as a function of z , which is transferred to TITAN.

6. Some applications

A full grid of models will be published elsewhere (Dumont & Abrassart 2000). Here we discuss only a few interesting cases.

6.1. Optically thin hot medium: the Warm Absorber in AGN

The Warm Absorber (WA) is a hot medium located on the line of sight of the X-ray source in AGN. It is responsible of the absorption edges of OVII and OVIII observed in their soft X-ray spectrum in about 50% of them. It might also constitute the “mirror” invoked in the Unified Scheme to account for the polarized Broad Lines observed in Seyfert 2 galaxies (Antonucci & Miller 1985). It has been modelled in many papers, using ION (Netzer 1993, 1996), XSTAR (Krolik & Kriss 1995), CLOUDY (Nicastro, Fiore & Matt 1999 for the most recent paper), PEGAS and IRIS (Porquet et al. 1999). This medium has a column density of 10^{21} to 10^{24} cm $^{-2}$, and a typical illumination parameter of $\xi = 100$ erg cm s $^{-1}$. Porquet et al. have shown that its density should be at least 10^{10} cm $^{-3}$ to avoid the emission of too strong coronal lines.

As the WA is relatively thin ($\tau_\nu \ll 1$ for the continuum in a large range of frequencies), it is possible to use the line escape probability formalism. This is however limited to the case where τ_ν is smaller than unity in the continuum underlying intense lines. This specific problem will be discussed in detail in the paper describing the code PEGAS (Dumont & Porquet 2000). A correct computation of the backward flux is also required. We have shown indeed that the temperature depends on the intensity of this backward flux.

We have run several models corresponding to the conditions of the WA, i.e. for $\xi = 100$ erg cm s $^{-1}$ and column densities varying from 10^{22} to 10^{24} cm $^{-2}$ (the other parameters being the same as in the reference model). We have compared the results to those obtained with CLOUDY for the same models, to check that they are similar at low column densities, and to determine at which column densities they begin to differ strongly. Note that a detailed comparison between TITAN and CLOUDY is not possible, as these codes differ both in the transfer method and in the atomic data (for instance owing to the semi-isotropic illumination, a given column density corresponds to a larger optical thickness with TITAN than with CLOUDY), so only trends can be obtained.

Fig. 14 displays the dependence of the temperature on z , obtained with TITAN and with CLOUDY. As discussed previously, it is higher with TITAN at the illuminated side for a high column density, owing to the returning flux, and it is lower at the dark side.

The ionization state (of fundamental importance for the study of the WA) and the emission spectrum, are also

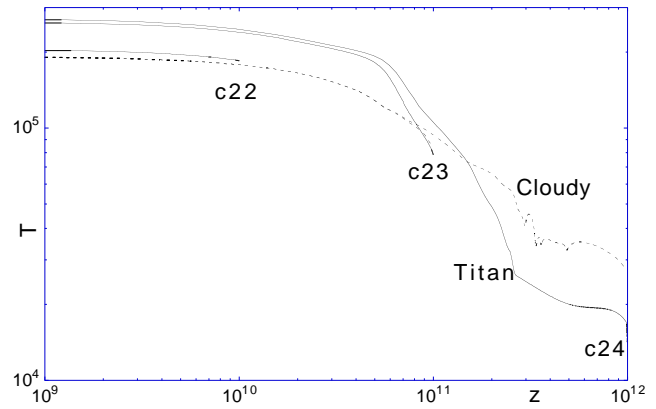


Fig. 14. Dependence of the temperature in K on the distance to the illuminated side, for $\xi = 100$ erg cm s $^{-1}$ and column densities varying from 10^{22} to 10^{24} cm $^{-2}$. The temperature obtained with CLOUDY is shown for comparison.

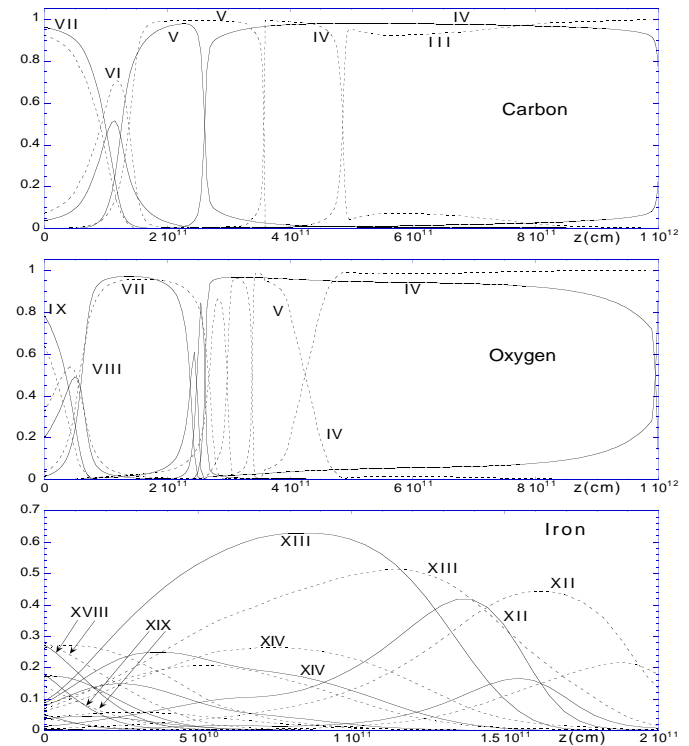


Fig. 15. Fractional abundances of Carbon, Oxygen, and Iron, computed by TITAN (full lines) and CLOUDY (dashed lines), as functions of the distance to the illuminated side, for $\xi = 100$ erg cm s $^{-1}$ and a column density equal to 10^{24} cm $^{-2}$. Note that the abscissa scale for Iron differs from the others.

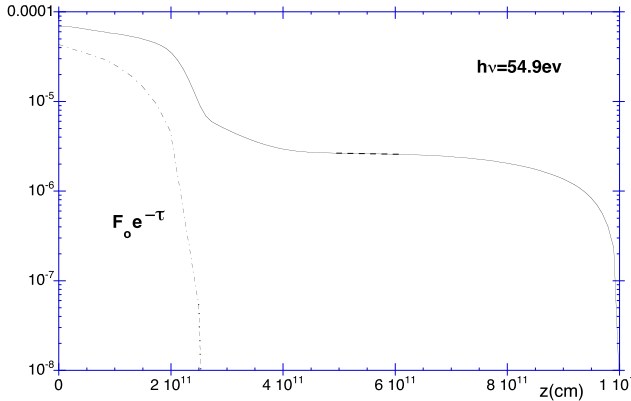


Fig. 16. Variation of the flux at 54.9 eV (the OIII-OIV ionization edge) as a function of the depth, and comparison with the transmitted flux.

different with TITAN and with CLOUDY at high column densities. Fig. 15 shows the ionization state of Carbon, Oxygen and Iron for a column density of 10^{24} cm^{-2} , computed with TITAN and with CLOUDY. While the ionization state close to the illuminated side is quite similar (in particular if one remembers that there is a factor $\sqrt{3}$ in the optical depth), it is very different in the deepest layers, where CLOUDY leads to a smaller degree of ionization than TITAN (CIII and OIII instead of CIV and OIV). This effect cannot be explained by the difference in optical thickness, which acts in the opposite direction. It is certainly due to the different treatments of the diffuse continuum, and perhaps of the lines. With TITAN we have checked that the diffuse continuum at large depths is sufficient to ionize OIII into OIV. To illustrate this point Fig. 16 displays the variation of the flux at 54.9 eV (the OIII-OIV ionization edge) as a function of the depth. It shows that the diffuse flux is still very intense and sufficient to ionize OIII at large depths (contrary to the transmitted flux which is very weak). Note that this result *depends strongly on the way the spectral distribution of the diffuse flux is computed*. If it would be reduced to a unique frequency at the recombination frequency of He^{++} , 54.4 eV, (as it is generally the case with the “On The Spot” approximation), there will be no photons able to ionize OIII.

Fig. 17 displays the reflected and outward spectra, for column densities 10^{23} and 10^{24} cm^{-2} . We see that the overall shape of the continuum is very similar with TITAN and with CLOUDY. However, some differences in the detailed features appear for the largest column density. For instance the Lyman edge is in emission in the reflected spectrum with both codes, but it is larger with TITAN (presumably because the temperature is higher in the emission layers). In the outward spectrum it is present as a very weak absorption with CLOUDY, while it is in emission with TITAN.

The line spectra are obviously also different. There are much more lines with CLOUDY, but on the other hand the

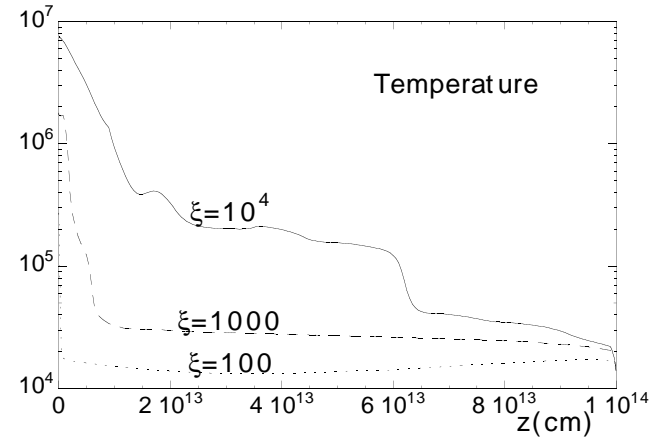


Fig. 18. Temperature in K versus z for different values of ξ in erg cm s^{-1} , the other parameters being the same as in the reference model.

fewer lines of TITAN are more intense. This is expected since subordinate lines are not taken into account except for hydrogen-like ions in TITAN. As mentioned before, some lines appear in absorption with TITAN, both in the reflected and in the outward spectrum.

6.2. Hot medium optically thick to Compton scattering: the UV-soft X-ray emitting medium in AGN

TITAN is specially designed for Compton thick photoionized media like those commonly assumed to emit the UV/soft X-ray continuum in AGN and to produce through Compton reflection the FeK ~ 7 KeV line and the 30 KeV hump observed in many Seyfert 1 galaxies.

Although the exact nature of this medium is not known (an irradiated accretion disc, as proposed by Ross & Fabian 1993, Zycki et al. 1994, to quote only the first papers on the subject, or a clumpy Compton thick medium, cf. Collin-Souffrin et al. 1996), its characteristics and physical state are comparable: a shell of gas with a column density of at least 10^{25} cm^{-2} , a temperature of $10^5\text{--}10^6 \text{ K}$ due to radiative heating, and a density spanning a range from 10^{12} to 10^{15} cm^{-3} . The corresponding value of ξ is typically 300 to 3000 erg cm s^{-1} . Our reference model is therefore representative of this medium. In the case of an irradiated accretion disk, it has been mimicked as a shell of constant density irradiated from above by a power law continuum, and from below by a black body radiation (actually it is not the best way to take into account the presence of the underlying viscously heated disk, cf. Rozanska et al. 2000).

Let us consider first a slab illuminated on one side by a semi-isotropic radiation. Fig. 18 displays T versus z , for different values of ξ . The other parameters are the same as in the reference model. It is interesting to notice that the quasi constant temperature regime (corresponding to LTE) is reached for increasing values of z when ξ increases.

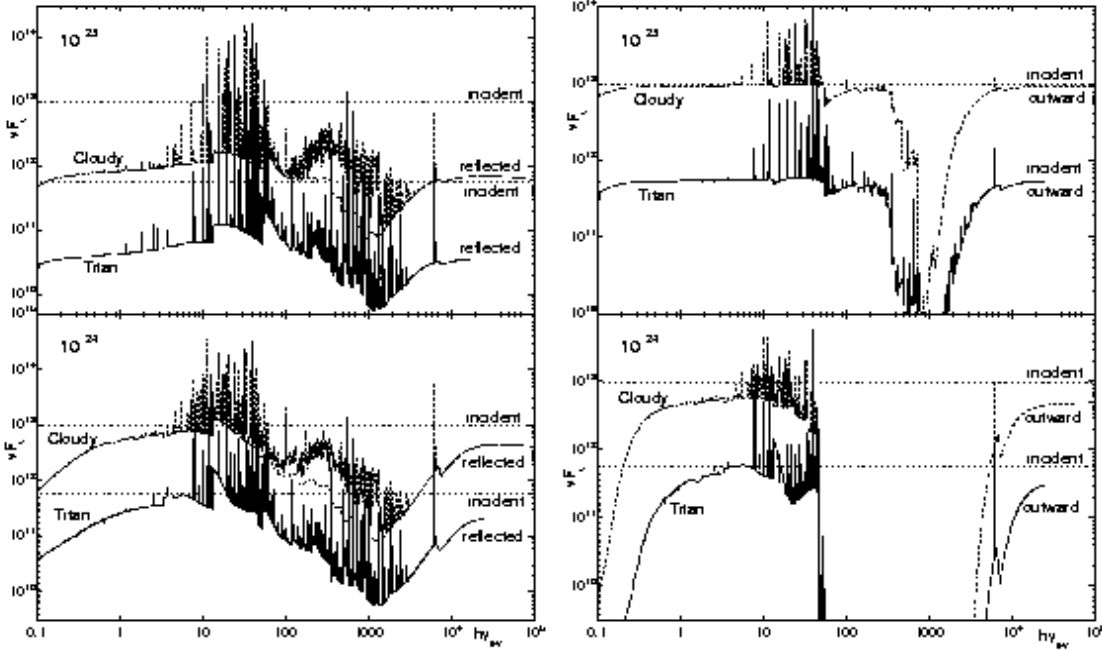


Fig. 17. Reflected and outward spectrum, for $\xi = 100 \text{ erg cm s}^{-1}$ and column densities equal to 10^{23} and 10^{24} cm^{-2} . The results obtained with CLOUDY are shown for comparison in dashed lines. The incident flux of CLOUDY is multiplied by a factor $\sqrt{3}$ to account for the semi-isotropy of the intensity in TITAN, and the emitted fluxes are multiplied by an additional factor 10 for a better visibility. The spectra are displayed with a line resolution of 300.

For instance it is reached for $z \sim 10^{13} \text{ cm}$, corresponding to $\tau_T \sim 6$ for $\xi = 1000 \text{ erg cm s}^{-1}$. It means that any computation aiming at giving the reflected spectrum of such a model should *solve correctly the thermal and ionization equilibrium until these deep layers*.

Fig. 19 shows the reflected spectrum for the same models. Note that the resolution adopted here (100) does not correspond to a region where the lines are broadened by large velocity field, either turbulent or organized (rotation). We use this high resolution only to show more clearly the details of the spectrum.

We see that the overall shape of the spectrum computed with TITAN and NOAR is very similar in the range 1-20 KeV. However the detailed spectral features are different, particularly for the higher values of ξ . For instance the complex feature near 7 KeV (which is made of a mixture of several Iron edges and of Iron lines dominated by low ionization stages for $\xi = 100 \text{ erg cm s}^{-1}$, and by FeXXV and FeXXVI for $\xi = 10^4 \text{ erg cm s}^{-1}$) is strongly modified by Compton scattering. For $\xi = 10^4 \text{ erg cm s}^{-1}$ the line has a large red wing due to direct Compton scattering, and a weak blue wing due to inverse Compton scattering. The absorption edge is also completely erased. The effect is smaller for $\xi = 10^3 \text{ erg cm s}^{-1}$, and almost absent for $\xi = 100 \text{ erg cm s}^{-1}$, as discussed above. Similar results have been obtained in many papers dealing with the X-

ray spectrum of Seyfert galaxies (cf. for instance Ross et al. 1999).

Let us now compare the results obtained by us with TITAN, and by Zycki et al. (1994), for a slab of constant density 10^{14} cm^{-3} , illuminated by a power law $\nu^{-0.9}$ between 10 eV and 100 KeV on one side, and by a black body $T_{\text{BB}} = 10^5 \text{ K}$ on the other side. We will compare the results for ξ (Zycki et al.)=300, which corresponds to ξ (TITAN) $\sim 200 \text{ erg cm s}^{-1}$, owing to our semi-isotropic illumination, and to a slightly different definition of ξ .

Like us, Zycki et al. used a Monte-Carlo method to take into account Compton scattering. The thermal and ionization state of the gas is calculated apart with the code XSTAR, using like CLOUDY the escape probability approximation. Fig. 20 gives T versus τ_T obtained by us and by Zycki et al. The same result is observed as with CLOUDY: our temperature is larger near the surface of the slab. It reaches T_{BB} at $\tau_T=0.7$. For a larger value of ξ , the connection with the underlying black body would be reached in even deeper layers, as discussed above. For $\tau_T \geq 0.7$ the temperature becomes smaller than T_{BB} , and joins T_{BB} only at $\tau_T \sim 20$. This behaviour is however dependent on the thickness of the slab, it is why this representation of the disk is not meaningful (Rozanska et al. 2000). On the contrary Zycki et al. impose the gas temperature to be equal to $\min(T_{\text{BB}}, T_{\text{thermal balance}})$.

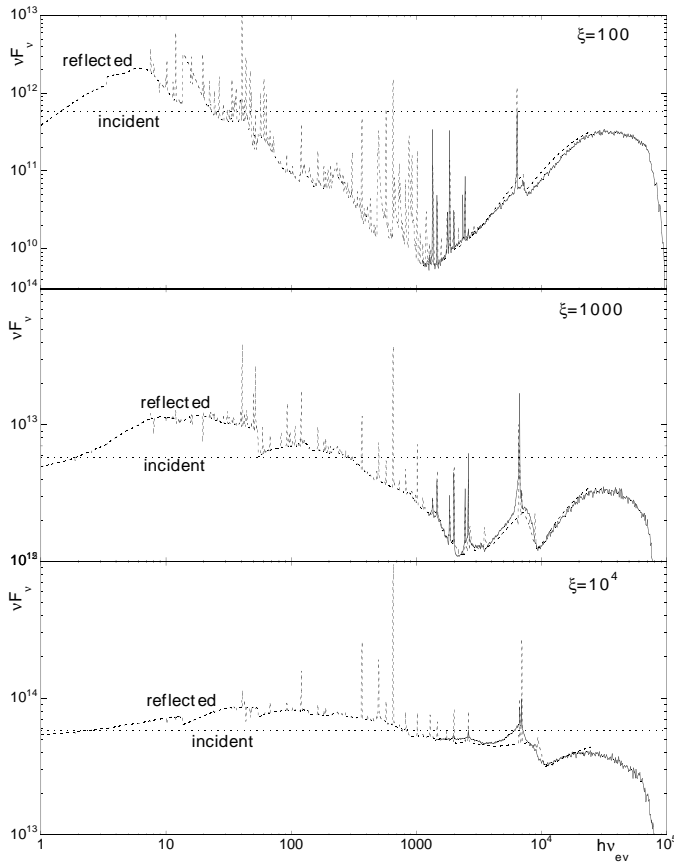


Fig. 19. Reflected spectrum for different values of ξ in erg cm s^{-1} , the other parameters being the same as in the reference model; full lines: results of NOAR; dashed lines: results of TITAN. The spectra are displayed with a resolution of 100.

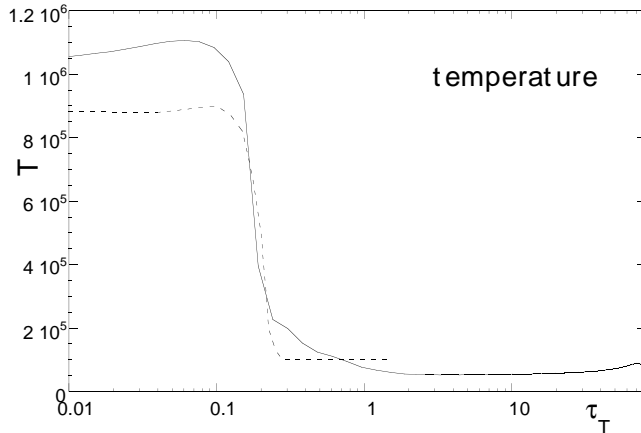


Fig. 20. Temperature in K versus τ_T for the “accretion disk” model (see text), computed by us (full line), and by Zycki et al. (dashed line).

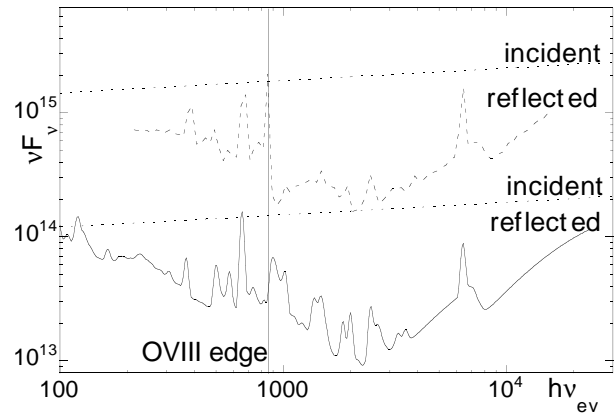


Fig. 21. Reflected spectrum for the “accretion disk” model computed by us (full line), and by Zycki et al. (dashed line). Zycki et al. spectrum is shifted for clarity. The resolution is 20 for the TITAN spectrum.

Fig. 21 displays the reflected spectrum, computed by us and by Zycki et al. The resolution is degraded to 20, to fit the energy bins of Zycki et al. The overall shape of the spectra are roughly similar. The major discrepancy is the OVIII edge, in emission with our computation and in absorption with Zycki et al.’s one. We think that it is due to the higher surface temperature and to the lower temperature in the deeper layers obtained in our computation.

7. Conclusion

We have shown that the coupling of TITAN and NOAR allows to compute the structure and the emission of hot Compton thick irradiated media in an unprecedented way. First it solves consistently both *the global and the local* energy balance, which is impossible in a thick medium with codes handling the line transfer with the escape probability approximation, as all present photoionization codes do. We have also shown the importance of the returning flux (which is neglected in photoionization codes) even for relatively low column densities. Second it takes into account in an exact way inverse and direct Compton scattering, both in the energy balance and in the computation of the emitted spectrum. Finally, it allows to treat any geometry, open or closed.

Although the problem of the convergence process is not as drastic as in stellar atmospheres, since we are able to get complete converged structure and spectrum in a still reasonable computing time, a most urgent improvement of the code is to accelerate the convergence process through the use of the Accelerated Lambda Iteration method. This will not only allow to get the results in a much smaller time, but also to get convergence for the few lines which are still not converged after about 10^3 iterations.

Then the following improvements of TITAN will be to take into account subordinate lines in solving a multi-level

atom for all ions and to bring up to date the atomic data. More detailed line spectra for some abundant ions will be obtained through coupling with the code IRIS. The L shells of Iron which are already taken into account for FeXVII to FeXXII will be implemented as well as a better representation of the Iron K lines. A few elements will be added to the already ten existing ones.

Acknowledgements. We are grateful to the referee, G. Ferland, for his comments which have led to substantially clarify the paper, to M-C. Artru for a very careful reading of the manuscript, and to I. Hubeny for enlightning discussions.

References

Abrassart A., 1999, in Proceedings of the 32nd Cospar Scientific Assembly, Nagoya, Japan, Advances in Space Research, Vol 25 issue/3-4, p 465

Abrassart A., 2000, Ph.D. thesis, University of Paris XI, in preparation

Aldrovandi S., Péquignot D., 1973, A&A 25, 137

Allen C.W. 1973, "Astrophysical quantities", University of London, The Athlone Press

Antonucci R.R.J., Miller J.S., 1985, ApJ 297, 621

Arnaud M., Raymond J., 1992, ApJ 398, 394

Avrett E.H., Loeser R., 1988, ApJ 331, 211

Band L.M., Trzhaskovskaya M.B., Verner D.A. and Yakovlev D.G., 1992, A&A 237, 267

Band D.L., Klein R.I., Castor J.I. and Nash J., 1990, ApJ 362, 90

Bergeron J., Souffrin S., 1973, A&A, 25, 1

Canfield R.C., Ricchiazzi P.J., 1980, ApJ 239, 1036

Coleman H.H., 1993, Ph.D. thesis

Collin-Souffrin S., Delache P., Dumont S., Frisch H., 1981, A&A 104, 264

Collin-Souffrin S., Dumont S., 1986, A&A 166, 13

Collin-Souffrin S., Czerny B., Dumont A-M., Zycki P., 1996, A&A 314, 393

Czerny B., Dumont A-M., 1998, A&A 338, 386

Daresbury Report, 1985, "Daresbury Atomic Data Workshop", March 1985

Dumont A-M., Abrassart A., 2000, in preparation

Dumont A-M., Porquet D., 2000, in preparation

Elitzur M., Netzer H., 1984, ApJ 291, 464

Ferland G.J., Rees M.J., 1988, ApJ 332, 141

Ferland G.J., 1996, HAZY, "a brief introduction to Cloudy", University of Kentucky, Dept of Physics and Astronomy, Internal Report

Ferland G.J., Korista T., Verner D.A., Ferguson J.W., Kingdom J.B., Verner E.M., 1998, PASP 110, 761

Fuhr J.R., Martin G.A. and Wiese W.L., 1988, Journ. of Phys. and Chem. Reference Data

Gorecki A. & Wilczewski W. 1984, Acta Astronomica, 34, 141

Hubeny I., 1990, ApJ 351, 632

Hubeny I., 1997, "Stellar Atmosphere Theory: An Introduction", Lectures given at the 9th European Doctoral School.

Hubeny I., Hubeny V., 1997, ApJ 484, L37

Hubeny I., Hubeny V., 1998, ApJ 505, 558

Kallman T.R., McCray R., 1982, ApJ Suppt 50, 263

Kallman T.R., Krolik J.H., 1995, "XSTAR, a Spectral Analysis Tool, Version 1.20 of the "Users Guide"

Kaastra J.S., Mewe R., 1993, AAPS 97, 443

Ko Y.-K., Kallman T.R., 1994, ApJ 431, 273

Krolik J.H., Kriss G.A., 1995, ApJ. 447, 512

Kwan J., Krolik J.H., 1981, ApJ 250, 478

Lightman A., White T., 1988, ApJ 335, 57

Matt G., Fabian A.C., Ross R.R., 1993, MNRAS 264, 839

Martocchia A., Matt G., 1996, MNRAS 282, L53

Mewe R., 1972, A&A 20, 215

Mihalas D., 1978, "Theory of stellar atmospheres", San Francisco : Freeman Edt.

Netzer H., Elitzur M., Ferland G.J., 1985, ApJ 299, 752

Netzer H., 1990, in "Active Galactic Nuclei", Blanford R.D., Netzer H., Woltjer L., Eds. Courvoisier T., Mayor M., Springer-Verlag Berlin, New York

Netzer H., 1993, ApJ 411, 594

Netzer H., 1996, ApJ, 473, 781

Nicastro F., Fiore F., Matt G., 1999, ApJ 517, 108

Porquet D., Dumont A-M., Collin S., Mouchet M., 1999, A&A 341, 58

Pozdniakov L.A., Sobol I.M. & Sunyaev R.A., 1983, Astrophysics and Space Physics Reviews, 2, 189

Rees M.J., Netzer H., Ferland G.J., 1989 ApJ 347, 640

Reilman R.F., Manson S.T., 1979, ApJ Suppt 40, 815

Ross R.R., 1979, ApJ 233, 334

Ross R.R., Fabian A.C., 1993, MNRAS 261, 74

Ross R.R., Fabian A.C., Young A.J., 1999, MNRAS 306, 461

Rozanska A., Czerny B., Dumont A-M., 2000, in preparation

Rutten R.J., "Radiative Transfer in Stellar Atmospheres", 2nd WWW edition, 1995, Robert J. Rutten, Utrecht, Netherlands

Zycki P.T., Krolik J.H., Zdziarski A.A., Kallman T.R., 1994, ApJ 437, 597

Zycki P.T., Czerny B., 1994, MNRAS 266, 653

Appendix : Previous methods

7.1. Transfer of the continuum

It is not always clear which approximations are used in the different codes. Basically the computation of the diffuse radiation field seems to be similar in all codes, except in Ross & Fabian (1993) and in subsequent works using this code, where it is computed using the Kompaneets equation. CLOUDY (Ferland 1996), XSTAR (Kallman & Krolik, 1995 for the last version), ION (Netzer 1990, 1993), use a modified version of the "on the spot" approximation, which amounts to assuming a kind of escape probability for the diffuse continuum, and one stream approximation in the transfer equation. These approximations are correct only for a continuum optical thickness smaller than unity (effective or total opacity), and when the properties of the cloud do not vary considerably between the point where a photon is emitted and the point where it is reabsorbed. In particular one very important requirement for studying hot and thick media is to take into account the radiation returning from the backside of the slab, even when it is not

illuminated. As the medium is optically thick in a large frequency range, this radiation is intense and modifies the physical state of the whole slab, including the illuminated side (see Fig. 2).

7.2. Line transfer: the escape probability approximation

All previous photoionization codes, except that of Collin-Souffrin and Dumont (S.) (1986), treat line transfer by the so-called local escape probability formalism, which uses the probability that a line photon emitted at a given point can escape **in a single flight** from the cloud, assuming that the rest of the cloud is homogeneous and has the same properties as the emitting layer. It amounts to identifying the divergence flux of the statistical equilibrium equations with the escape probability intervening in the line emerging flux. This approximation is valid only in the case of complete frequency redistribution, absence of line interlocking, and **if the medium is homogeneous**. Its use can have severe consequences on the emission line spectrum and on the energy balance when these conditions are not fulfilled as it was often discussed, see for example by Collin & S.Dumont (1986) or Elitzur (1984). We introduce here the divergence flux in the aim to show that our results are completely different from those obtained by the escape probability formalism.

To simplify the discussion, let us consider in the rest of this section a simple two-level atom. The level population balance writes:

$$\begin{aligned} n_u(A_{ul} + B_{ul} \int J_\nu \psi_\nu d\nu + n_e C_{ul}) \\ = n_l(B_{lu} \int J_\nu \phi_\nu d\nu + n_e C_{lu}) \end{aligned} \quad (16)$$

where ϕ_ν and ψ_ν are the absorption and emission line profiles, A_{ul} , B_{ul} and B_{lu} , C_{ul} and C_{lu} are the usual radiative (Einstein) and collisional excitation and deexcitation coefficients, and J_ν is the angle averaged intensity.

Let us now define the *divergence flux* of the transition, ρ_{ul} :

$$\rho_{ul} = \frac{\{n_u(A_{ul} + B_{ul} \int J_\nu \psi_\nu d\nu) - n_l(B_{lu} \int J_\nu \phi_\nu d\nu)\}}{n_u A_{ul}}. \quad (17)$$

With this definition Eq. 17 becomes simply:

$$n_u (n_e C_{ul} + \rho_{ul} A_{ul}) = n_l n_e C_{lu}. \quad (18)$$

Let us assume *the line is the only contributor to radiation*. The energy emitted locally in the line in a small volume of surface 1 cm^{-2} and length dz writes:

$$\begin{aligned} dF = h\nu [n_u(A_{ul} + B_{ul} \int J_\nu \psi_\nu d\nu) - n_l B_{lu} \int J_\nu \phi_\nu d\nu] dz \\ = \rho_{ul} n_u A_{ul} h\nu dz = \rho_{ul} 4\pi \epsilon dz \end{aligned} \quad (19)$$

where ϵ is the emissivity coefficient $n_u A_{ul} h\nu / 4\pi$. Integrating this equation over depth, one gets the emerging line flux:

$$F = 4\pi \int \rho_{ul} \epsilon dz \quad (20)$$

According to this equation the divergence flux seems to be equal to the probability that, once emitted at a distance z from the surface, a photon can escape from the medium, which is called the “escape probability” P_e .

From this fact, if one makes *the approximation that the emission and the absorption profiles are equal*, one computes this escape probability by integrating the attenuation over the line profile:

$$P_e \sim \frac{1}{2} \frac{\int_0^1 \int \frac{h\nu}{4\pi} n_u A_{ul} \phi_\nu \exp(-\tau \phi_\nu / \mu) d\nu d\mu}{\int \frac{h\nu}{4\pi} n_u A_{ul} \phi_\nu d\nu} \quad (21)$$

where $\mu = \cos\theta$, and it gives the usual expressions for complete redistribution in a Voigt profile:

$$P_e(\tau_0) \sim \max \left(\frac{1}{1 + 2\tau_0 \sqrt{\pi \ln(\tau_0 + 1)}}, \frac{2}{3} \sqrt{\frac{a}{\tau_0 \sqrt{\pi}}} \right), \quad (22)$$

where τ_0 is the optical thickness at the line center and a is the usual damping constant. This expression can thus replace ρ_{ul} in Eqs. 18 and 20.

With this method the frequency dependent transfer equations are successfully replaced by frequency integrated ones, and solved consistently with the statistical equations.

Several estimates of the escape probability are used in the literature (see for example Kwan & Krolik, 1981, Rees, Netzer & Ferland, 1989, Kallman & McCray, 1982, Ko & Kallman, 1994), to account for partial redistribution, for line or continuum interlocking, and for continuum absorption. For instance several ways to take into account the continuum opacity (or the overlapping of two lines) have been proposed (Elitzur & Netzer, 1984, Netzer, Elitzur & Ferland, 1985). In the case of the Broad Line Region of AGN, which is optically thin for the continuum underlying the main lines, Collin-Souffrin et al. (1981), Avrett & Loeser (1988), have discussed the influence of different approximations for partial or complete redistribution, and how they compare to an exact transfer treatment, and Collin-Souffrin & Dumont S. (1986) have shown that the escape probability approximation is roughly valid (it can however lead to a decrease by a factor as large as two of the ratio of a lower to a higher transition, such as H α /H β or L α /H α).

However these approximations are not valid if τ_{cont} is of the order of unity at the line frequency and if the line photons are created in one place and absorbed in another place where the physical conditions are different. This happens for instance for EUV and soft X-ray lines created in the hot region and absorbed in ionizing He $^+$ ions in a cooler region.

If the local escape probability approximation breaks down, it has a severe consequence: *the emitted line spectrum and the thermal and the ionization balance are not correctly computed*. For instance the divergence flux takes frequently negative values in our computations, even for intense lines, and even in the reflected spectrum. This is not allowed with escape probabilities. We illustrate this discussion with some examples in Sect. 3.2.